Materials Science Forum Vol. 508 (2006) pp 193-198
Online available since 2006/Mar/15 at www.scientific.net
© (2006) Trans Tech Publications, Switzerland
doi:10.4028/www.scientific.net/MSF.508.193

Gravity-Induced Convection during Directional Solidification of Hypermonotectic Alloys

A. Ludwig[1], M. Wu[1,a], M. Abondano[2] and L. Ratke[3]

[1]Dept. of Metallurgy, Univ. of Leoben, A-8070 Leoben, Austria

[2]Foundry Institute, Technical University of Aachen, D-52072 Aachen, Germany

[3]German Aerospace Research Center DLR, D-51140 Cologne, Germany

[a]menghuai.wu@notes.unileoben.ac.at

Keywords: Hypermonotectic, decomposition, directional solidification, modeling, droplet motion, convection, phase distribution.

Abstract. A two-phase volume-averaging model developed for the simulation of the dynamic decomposition and solidification of hypermonotectic alloys was used to study the occurrence of convection phenomena during directional solidification of a hypermonotectic alloy (Al-10 wt.%Bi) under terrestrial condition. The model accounts for nucleation and growth of secondary phase droplets, Marangoni and Stokes forces, solute partitioning, heat release due to decomposition and solidification. It is shown that the appearance and growth of secondary droplets is accompanied with a continuous downwards motion of droplets, which rapidly becomes unstable. After relaxation of this dynamic motion the advancing solidification front freezes in the resulting non-uniform droplet distribution.

Introduction

The components of the hypermonotectic alloy Al-10 wt.%Bi are completely miscible above the binodal. As the temperature drops in the miscibility gap, the minority liquid phase in spherical morphology (droplet) decomposes from the parent melt. This decomposition process includes nucleation and droplet growth (or coarsening). As the temperature further drops to below monotectic point T_m, monotectic reaction occurs, and the droplets of the minority phase will be entrapped in the monotectic matrix. For the industry applications, the ideal situation is that the soft minority phase must be dispersively distributed in the hard monotectic matrix. However, a macroscopic spatial redistribution of the minority phase seems unavoidable no matter whether the alloy solidifies under normal terrestrial condition [1-2] or under reduced gravity situation [3-5]. Two mechanisms are responsible for this phenomenon: the gravity induced sedimentation and the Marangoni (thermocapillary) motion. A two phase volume-averaging model, based on the Beckermann's [6-12] and Ludwig and Wu's previous works [13-15] on equiaxed solidification, was developed to model both the gravity-induced sedimentation and Marangoni motion of the secondary liquid droplets during hypermonotectic solidification [16-18]. This paper tries to use the same model to investigate the directional solidification of the hypermonotectic alloys. The goal is to achieve basic understanding to the dynamic processes of the droplet motion and the resulting melt convection, and their influence on the final phase distribution.

Short Description of the Numerical Model

At least 4 phases appear in hypermonotectic solidification: the parent melt ($L=L_1$), the decomposed secondary liquid phase (L_2), the solidified monotectic matrix (as one phase) and the solidified secondary phase. The recent model considers only two phases: the first liquid phase L_1 and the second liquid phase L_2. During monotectic reaction the monotectic matrix is transformed directly from L_1. Therefore the solidified monotectic matrix is modeled as L_1 phase in such a way that an enlarged viscosity is applied to the L_1 phase on reaching the monotectic temperature, and the latent heat of the monotectic reaction is added to L_1 phase. The L_2 droplets approaching the monotectic reaction front are modeled to be entrapped in the monotectic matrix by applying a similar enlarged viscosity at/below the monotectic point. In addition to the above phase definition, following assumptions are made:

(1) Gravity induced sedimentation is modeled with Boussinesq approach;
(2) Both liquid phases have same viscosity;
(3) Eutectic reaction of L_2 is ignored;
(4) Diffusion in a single droplet is infinitive, and between droplets is ignored.

The mathematical equations used for this two-phase hypermonotectic solidification system are summarized in Table 1. The subscripts 1 and 2 stand for L_1 and L_2 phases. Nucleation law for L_2 droplets is implemented in the source term N_n (nucleation rate). A simple coagulation model is also implemented to consider the reduction of the droplet number density N_w by the coagulation effect. Growth (or dissolution) of the L_2 phase is taken into account in Eq. 6 through a mass transfer term M_{12} (= $-M_{21}$). The gravity induced sedimentation is modelled with Boussenesq approximation. Nomenclature of Table 1, derivation of the numerical model, and numerical implementation of the model are described in previous publications [16-17].

Table 1: Conservation equations, exchange and source terms, and some auxiliary equations

Conservation equations

Mass:

$$\frac{\partial}{\partial t}(f_1\rho_1)+\nabla\cdot(f_1\rho_1\vec{u}_1)=M_{21} \tag{1}$$

$$\frac{\partial}{\partial t}(f_2\rho_2)+\nabla\cdot(f_2\rho_2\vec{u}_2)=M_{12}$$

Momentum:

$$\frac{\partial}{\partial t}(f_1\rho_1\vec{u}_1)+\nabla\cdot(f_1\rho_1\vec{u}_1\otimes\vec{u}_1)=-f_1\nabla p+\nabla\cdot\bar{\bar{\tau}}_1+f_1\rho_1\vec{g}+\vec{U}_{21}-\vec{F}_M \tag{2}$$

$$\frac{\partial}{\partial t}(f_2\rho_2\vec{u}_2)+\nabla\cdot(f_2\rho_2\vec{u}_2\otimes\vec{u}_2)=-f_2\nabla p+\nabla\cdot\bar{\bar{\tau}}_2+f_2\rho_2\vec{g}+\vec{U}_{12}+\vec{F}_M$$

where $\bar{\bar{\tau}}_1=\mu_1 f_1\left(\nabla\cdot\vec{u}_1+(\nabla\cdot\vec{u}_1)^T\right)$ and $\bar{\bar{\tau}}_2=\mu_2 f_2\left(\nabla\cdot\vec{u}_2+(\nabla\cdot\vec{u}_2)^T\right)$

Species:

$$\frac{\partial}{\partial t}(f_1\rho_1 c_1)+\nabla\cdot(f_1\rho_1\vec{u}_1 c_1)=\nabla\cdot(f_1\rho_1 D_1\nabla c_1)+C_{21} \tag{3}$$

$$\frac{\partial}{\partial t}(f_2\rho_2 c_2)+\nabla\cdot(f_2\rho_2\vec{u}_2 c_2)=\nabla\cdot(f_2\rho_2 D_2\nabla c_2)+C_{12}$$

Enthalpy:

$$\frac{\partial}{\partial t}(f_1\rho_1 h_1)+\nabla\cdot(f_1\rho_1\vec{u}_1 h_1)=\nabla\cdot(f_1 k_1\nabla\cdot T_1)+Q_{21}+\Delta h_M \tag{4}$$

$$\frac{\partial}{\partial t}(f_2\rho_2 h_2)+\nabla\cdot(f_2\rho_2\vec{u}_2 h_2)=\nabla\cdot(f_2 k_2\nabla\cdot T_2)+Q_{12}$$

where $h_1=\int_{T_{ref}}^{T_1} c_{p(1)}dT+h_1^{ref}$ and $h_2=\int_{T_{ref}}^{T_2} c_{p(2)}dT+h_2^{ref}$

Droplets:

$$\frac{\partial}{\partial t}n+\nabla\cdot(\vec{u}_2 n)=N_n+N_w \tag{5}$$

Exchange/source terms

Mass:

$$M_{12}=n\cdot\pi d_2\cdot\rho_2\cdot\frac{D_1}{\Delta c_d}\cdot\Delta c\cdot f_1 \tag{6}$$

Nucleation:

$$N_n=\frac{dn}{d\Delta T}=\frac{n_{\max}}{\sqrt{2\pi}\cdot\Delta T_\sigma}\cdot e^{-\frac{1}{2}\cdot\left(\frac{\Delta T-\Delta T_N}{\Delta T_\sigma}\right)^2} \tag{7}$$

Coagulation:

$$N_w=-\Gamma\cdot f_2\cdot n \tag{8}$$

Momentum:

$$\vec{U}_{12}=\vec{U}_{12}^d+\vec{U}_{12}^p,\quad \vec{U}_{12}^p=\vec{u}^*\cdot M_{12},\quad \vec{U}_{12}^d=K_{12}(\vec{u}_1-\vec{u}_2) \tag{9}$$

where $$K_{12} = -\frac{1+3\mu_2/2\mu_1}{1+\mu_2/\mu_1} \cdot \frac{12 f_2}{d_2^2} \cdot \mu_1 \tag{10}$$

Species: $$C_{12} = C_{12}^d + C_{12}^p, \quad C_{12}^p = c^* \cdot M_{12}, \quad C_{12}^d \text{ neglected} \tag{11}$$

Enthalpy: $$Q_{12} = Q_{12}^d + Q_{12}^p, \quad Q_{12}^p = h^* \cdot M_{12}, \quad Q_{12}^d = H^* \cdot (T_1 - T_2) \tag{12}$$

Marangoni force: $$\vec{F}_M = -\frac{6}{(1+\mu_2/\mu_1)\cdot(2+k_2/k_1)} \cdot \frac{f_2}{d_2} \cdot \frac{\partial\sigma}{\partial T} \cdot \nabla T \tag{13}$$

where $$\frac{\partial\sigma}{\partial T} = -1.26 \cdot \sigma_0 \cdot \frac{1}{T_c} \cdot \left(1 - T/T_c\right)^{0.26} \tag{14}$$

Auxiliary terms

Droplet size: $$d_2 = \left(\frac{6 \cdot f_2}{\pi \cdot n}\right)^{\frac{1}{3}} \tag{15}$$

Mixture concentration: $$c_{mix} = \frac{c_1 \cdot \rho_1 \cdot f_1 + c_2 \cdot \rho_2 \cdot f_2}{\rho_1 \cdot f_1 + \rho_2 \cdot f_2} \tag{16}$$

Problem Configuration

The main experimental technique to study solidification behaviour of hypermonotectic alloys at DLR/Cologne is the power-down directional solidification method using the so-called ARTEMIS furnace. With this method a vertically mounted rod of, for example, hypermonotectic Al-Bi specimen is molten uniformly above the binodal, kept for a while to improve homogeneity and then solidified directionally by decreasing the temperature at the bottom with a constant rate, $\dot{T}_C$. The temperature at the top is first kept constant and then, after a given delay time, t_d, also reduced by a second rate, $\dot{T}_H$. Generally, the cooling rate at the bottom and at the top is chosen to be equal, $\dot{T}_C \cong \dot{T}_H$, to get a temperature gradient at the solid-liquid interface which can roughly be assumed to be constant.

With this background information about the experiment in mind, and consider the limitation of the recent numerical model and calculation capacity (computer hardware), a reduced 2D casting geometry is designed (Figure 1). The casting (100 x 50 mm^2) is meshed into volume elements of 2.5x2.5 mm^2. The boundary condition is given in Figure 1. The nucleation parameters for L_2 droplets are $n_{\max} = 10^{13}$ m^{-3}, $\Delta T_N = 20$ K, $\Delta T_\sigma = 8$ K. The coagulation coefficient Γ takes 1.0 (1/s). Other thermal physical properties and modeling parameters are referred to literature [16-17].

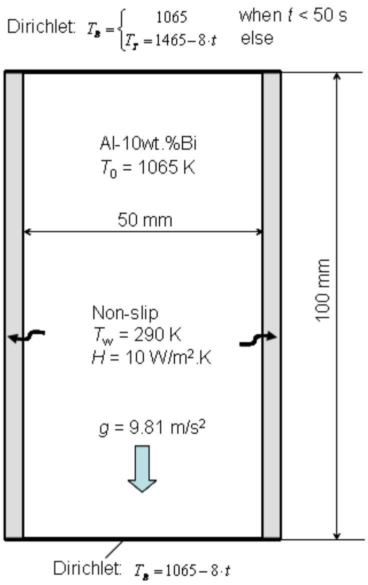

Figure 1. Scheme of the simulated case

Results

As result of the DS simulations, the appearance, growth and motion of the Bi-droplet together with the solidifying matrix is shown in Figure 2 with a sequence of 24 snapshots. The overall solidification time is numerically calculated to be 79 s. With 3 s of interval, the decomposition and solidification series from 3 s to 74 s are displayed in the Figure 2.

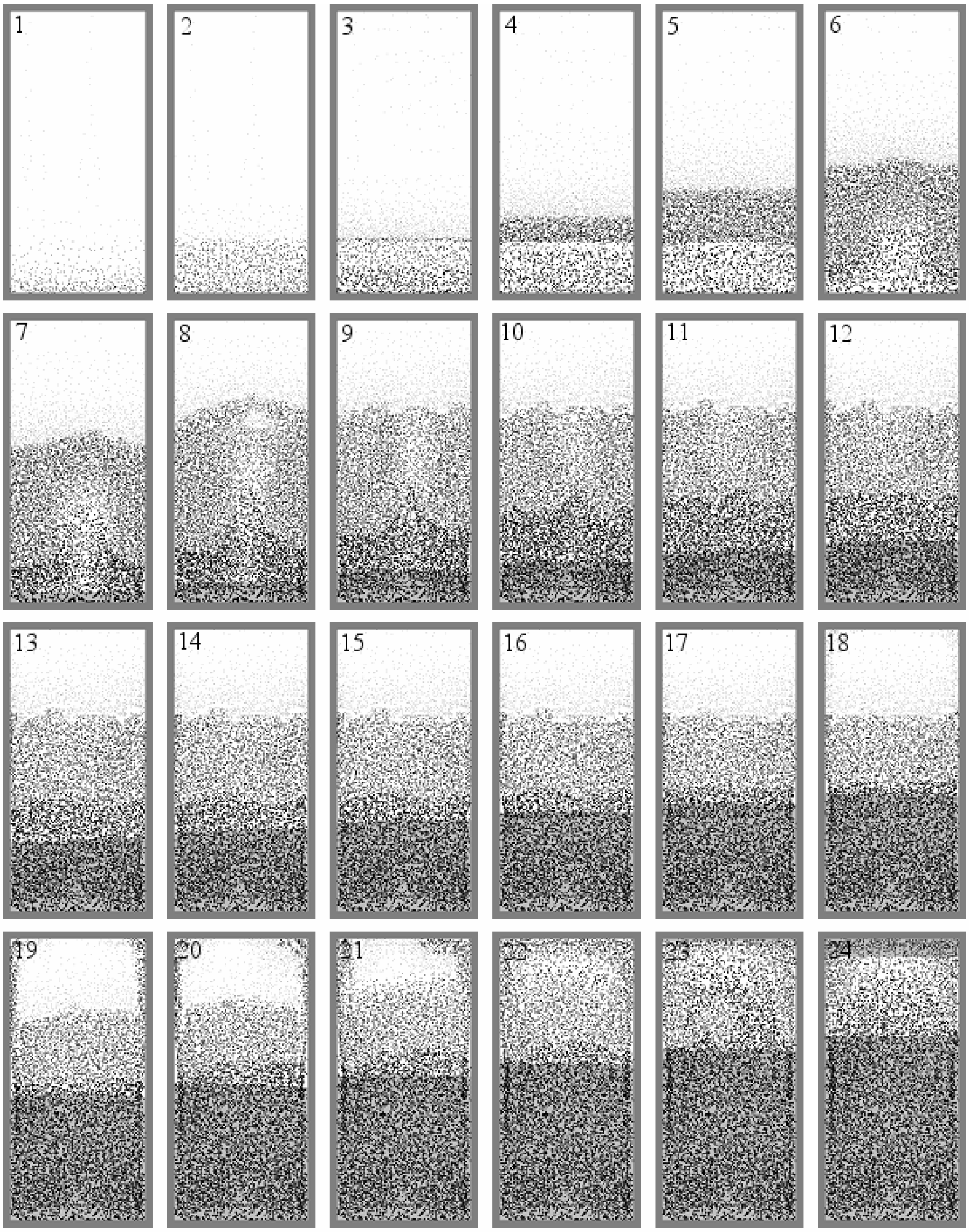

Figure 2: Formation of Bi droplets during directional solidification of hypermonotectic Al-Bi. Both the droplet density and the diameter of the droplets, shown in this figure, are reduced and enlarged by corresponding factors so that the droplet distribution can be seen with the naked eye.

Nucleation of Bi-droplets starts, according to Eq. 7, as soon as the temperature drops below the binodal. Due to the applied cooling conditions, this first happens at the bottom area of the rod. As soon as the Bi-droplets form, they start to submerge and sediment towards the bottom. While the Bi-droplets grow and sink, further nucleation leads to a continuous creation of new Bi-droplets above the already existing ones. The stratifying (layering) of droplets, visible in the first few pictures of Figure 2, is a result of the limited resolution of the post-processor and do not represent the numerical predictions properly. However, the higher droplet density appearing above the already existing droplets do reveal an improvement of the nucleation conditions caused by the establishment of a stronger temperature gradient and thus higher undercoolings.

The collective downwards movement of droplets has to be compensated by an upwards movement of parent melt. This relative motion is inherent instable, like for the classical Rayleigh-Bénard problem. As the downwards movement of droplets accelerates, the rising parent melt creates an upwards jet in the middle of the casting. The evolution of this instability can be seen in the pictures 6 to 8 of Figure 2. By this upwards jet of parent melt, some Bi droplets are carried from the bottom region into upper regions. However, due to their weight they tent to submerge again and calm down the parent melt jet slowly by momentum exchange. This calming down also flattens the boundary between the droplet-free area and the area filled with droplets, which had become irregular by the appearance of the upwards jet.

While this eruptive motion appears, further cooling at the bottom causes the parent melt to solidify at the monotectic temperature and so freeze-in the Bi-droplet. This is visualised by the grey area which propagate from the bottom upwards starting with the picture 7 of Figure 2. Note that the solidification front is not perfectly flat - a result of the convection-induced perturbations of isotherms. While the solidification front moves from below, the boundary between the droplet-free area and the area filled with droplets has become rather even again (picture 18).

In the meantime, cooling has also started at the top. Therefore, nucleation of Bi-droplets is now also possible at the top of the rod, especially at the top corner regions. The resulting droplets sink downwards along the right and left rod walls (picture 18 and following). This new source of Bi-droplets gets stronger and finally leads to the filling of the remaining areas with droplets.

Further cooling leads to the solidification of the parent melt at the monotectic temperature also from the top. Therefore, the final stage of solidification is characterized by two nearly flat monotectic fronts approaching each other. For the area where they finally meet, one can deduce that porosities may occur there.

As shown in Figure 3, the final solidification result shows the depletion of the primary L_2 phase in upper region (0.1 vol.%) and an enrichment of L_2 in the middle bottom region (11.6 vol.%). This result does not include the Bi phase in the monotectic matrix, that is 3.34 wt.% (0.858 vol.%). If taking this into account, the volume fraction of the Bi phase is about 0.958% at the top and 12.5% at the bottom.

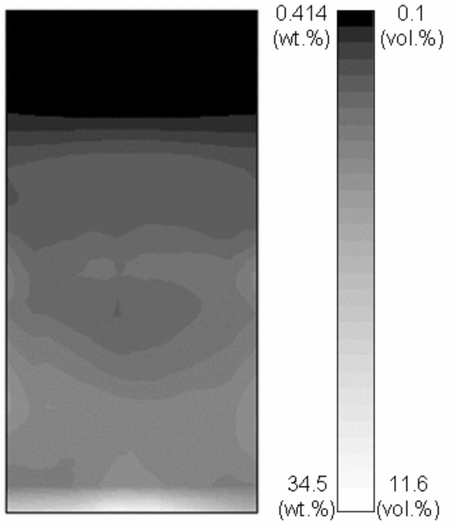

Figure 3. Prediction of the primary L_2 (Bi) phase distribution

Discussions and Conclusion Remarks

The above predicted phase separation phenomenon agrees with experiments performed by Alkemper and Ratke on a chilled cast Al-Bi alloys [2] and with those by Fujii et al on an Al-Pb-Bi ingot casting under normal terrestrial condition [19]: depletion of L_2 phase at the top of the sample and enrichment of L_2 phase at the bottom. For example, the Alkemper and Ratke's experiments with a 14 mm (diameter) x 20 mm (height) cylindrical sample (9.0~11.0 wt.%Bi alloys) show about 1.5 vol.% at the top and 9.5 vol.% at the bottom. Some modelling assumptions which influence the simulation accuracy have been discussed previously [16-17]: nucleation parameters, mesh quality, ignored solidification shrinkage, etc., but two points need to be specially mentioned here: one is the 3D characteristic of the real casting geometry which is reduced to 2D in the recent simulation; the other is the coagulation of the droplets, for which a simple model is used. Considering the geometrical difference of the samples used in the experiment and for the simulation, and the recent modelling assumptions, we find the experiment-simulation agreement is quite satisfactory.

It can be concluded that the two-phase model can be further developed as a numerical tool to study the hypermonotectic solidification including nucleation and growth of L_2 droplets, the gravity-induced and Marangoni-driven droplet motion, the melt convection, and their influences on the final L_2 phase distribution. Understanding to the microstructure evolution in hypermonotectic alloys with the dynamic effect of droplet motion and melt convection is achieved.

Acknowledgment

This work was/is supported by the ESA-MONOPHAS projects: first term "Solidification Morphologies of Monotectic Alloys" and second term "Advanced Bearing Alloys from Immiscibles with Aluminum". The authors also acknowledge Dr. M. Pelzer and Mr. U. Postl, Fluent Deutschland GmbH, Germany, for the technical assistance on FLUENT, Mr. Martin Feller, Foundry Institute Aachen, Germany, for his assistance to develop the post-processor.

References

[1] B. Prinz, A. Romero and L. Ratke: J. Mater. Sci. Vol. 30(1995), p. 4715

[2] J. Alkemper and L. Ratke: Z. Metallkd. Vol. 85 (1994), p. 365

[3] L. Ratke, G. Korekt and S. Drees: Adv. Space Res. Vol. 22 (1998, p. 1227

[4] L. Ratke and G. Korekt: Z. Metallkd. Vol. 91 (2000), p. 919

[5] H.U. Walter: *Proc. RIT/ESA/SSC Workshop: ESA SP 219* ed Järva Krog (Noordwijk, Sweden 1984), p. 47

[6] C. Beckermann and R. Viskanta: Appl. Mech. Rev. Vol. 46 (1993), p. 1

[7] J. Ni and C. Beckermann: Metall. Trans. Vol. 22B (1991), p. 349

[8] C.Y. Wang and C. Beckermann: Metall. Mater. Trans. Vol. 27A (1996), p. 2754

[9] C.Y. Wang and C. Beckermann: Metall. Mater. Trans. Vol. 27A (1996), p. 2765

[10] C.Y. Wang and C. Beckermann: Metall. Mater. Trans. Vol. 27A (1996), p. 2784

[11] C. Beckermann: JOM Vol. 49 (1997), p. 13

[12] A.V. Reddy and C. Beckermann: Metall. Mater. Trans. Vol. 28B (1997), p. 479

[13] A. Ludwig and M. Wu: Metall. Mater. Trans. Vol. 33A (2002), p. 3673

[14] M. Wu, A. Ludwig, P.R. Sahm and A. Bührig-Polaczek: *Proc. MCWASP X* ed D M Stefanescu et al (Warrendale, PA: Minerals, Metals and Materials Society 2003), p. 261

[15] M. Wu, A. Ludwig, A. Bührig-Polaczek, M. Fehlbier and P.R. Sahm: Inter. J. Heat Mass Transfer Vol. 46 (2002), p. 2819

[16] M. Wu, A. Ludwig and L. Ratke: Modell. Simu. Mater. Sci. Eng. Vol. 11 (2003), P. 755

[17] M. Wu, A. Ludwig and L. Ratke: Metall. Mater. Trans. Vol. 34A (2003), p. 3009

[18] M. Wu and A. Ludwig: Adv. Eng. Mater. Vol. 5, No.1 (2003), p. 62

[19] H. Fujii, T. Kimura, H. Kitaguchi, H. Kumakura and K. Togano: J. Mater. Sci. Vol. 30 (1995), p. 3429

Solidification and Gravity IV

doi:10.4028/www.scientific.net/MSF.508

Gravity-Induced Convection during Directional Solidification of Hypermonotectic Alloys

doi:10.4028/www.scientific.net/MSF.508.193